Finite-Element Formulation for Lossy Waveguides

KAZUYA HAYATA, KAZUNORI MIURA, AND
MASANORI KOSHIBA, SENIOR MEMBER, IEEE

Abstract —An efficient computer-aided solution procedure based on the finite-element method is developed for solving general waveguiding structures composed of lossy materials. In this procedure, a formulation in terms of transverse magnetic-field component is adopted and the eigenvalue of the final matrix equation corresponds to the propagation constant itself. Thus, one can avoid the unnecessary iteration using complex frequencies. To demonstrate the strength of the present method, numerical results for a rectangular waveguide filled with lossy dielectric are presented and compared with exact solutions. As more advanced applications of the present method, a shielded image line composed of a lossy anisotropic material and a lossy dielectric-loaded waveguide with impedance walls are analyzed and evaluated.

I. Introduction

COMPUTER-AIDED numerical analysis has become a necessary tool for designing microwave and optical waveguiding structures such as image line, microstrip line, optical channel guide, and optical fiber [1]. Increasing complexities of modern wave functional devices, particularly in monolithic integrated circuit form, have created a critical need for more accurate and efficient computer-aided analysis techniques.

Among several methods, the finite-element method (FEM) enables one to predict accurately the modal characteristics of a waveguide system with an arbitrary cross section. To date almost all of the applications of the FEM have been focused on a loss-free system. On the other hand, attempts have been made for a lossy system, using the axial electromagnetic-field (E_z-H_z) formulation [2]–[5] and the scalar approximation [6], [7].[1] However, they have some crucial drawbacks. In the E_z-H_z formulation, spurious solutions appear because of singularity of the operator and they are coupled with physical solutions. Furthermore, unnecessary iterations are involved until the imaginary part of complex frequency is negligible because the eigenvalue of the final matrix equation corresponds to the frequency. On the other hand, in the scalar approximation, spurious solutions do not appear and iterations are not involved. However, this approximation is applicable only to weakly guiding structures such as optical waveguides.

In this paper, an efficient computer-aided solution procedure based on the vectorial finite-element method is developed for solving general waveguiding structures composed of lossy materials. In this procedure, a formalism in terms of transverse magnetic-field component established for a loss-free system [10] is extended to a lossy system. The main advantage of this approach is that one can avoid the unnecessary iteration using complex frequencies because the eigenvalue of the final matrix equation to be solved corresponds to the propagation constant itself. To demonstrate the strength of the present method, numerical results for a rectangular waveguide filled with lossy dielectric are presented and compared with exact solutions. As more advanced applications of the present method, a shielded image line composed of a lossy anisotropic material and a lossy dielectric-loaded waveguide with impedance walls are analyzed and evaluated.

II. Basic Equations

We consider a three-dimensional dielectric waveguide with an arbitrary cross section Ω in the xy plane (Fig. 1), whose relative permittivity tensor $[\epsilon]$ is

$$[\epsilon]=\begin{bmatrix}\epsilon_x & 0 & 0\\ 0 & \epsilon_y & 0\\ 0 & 0 & \epsilon_z\end{bmatrix} \tag{1}$$

$$\epsilon_i=\epsilon_i'-j\epsilon_i'', \qquad i=x,y,z \tag{2}$$

where ϵ_i' and ϵ_i'' are the real and the imaginary part of the complex relative permittivity ϵ_i, respectively.

With a time dependence of the form $\exp(j\omega t)$ being implied, from Maxwell's equations the following vectorial wave equation is obtainable:

$$\nabla\times\left([\epsilon]^{-1}\nabla\times\boldsymbol{H}\right)-k_0^2\boldsymbol{H}=0 \tag{3}$$

where k_0 is the free-space wavenumber.

The divergence-free constraint $\nabla\cdot\boldsymbol{H}=0$ can be written

$$H_z=\gamma^{-1}\left(\partial H_x/\partial x+\partial H_y/\partial y\right) \tag{4}$$

where

$$\gamma=\alpha+j\beta. \tag{5}$$

Manuscript received April 23, 1987; revised August 21, 1987. This work was supported in part by Joint Research for Large-Scale Computations Using Vector Processor, Hokkaido University Computer Center, Sapporo, Japan.

The authors are with the Department of Electronic Engineering, Hokkaido University, Sapporo, 060 Japan.

IEEE Log Number 8717980.

[1] Recently, Matsuhara *et al.* [8] have extended the finite-element formulation in terms of the transverse electric and magnetic field components [9] to the waveguide with loss or gain.

0018-9480/88/0200-0268$01.00

Here, α, β, and γ are the attenuation, phase, and propagation constants, respectively.

III. Finite-Element Formulation

Dividing the cross section Ω of the guide into a number of second-order triangular finite elements as shown in Fig. 1, the magnetic fields within each element are defined in terms of those at the corner and midside nodal points:

$$\boldsymbol{H} = [N]^T\{H\}_e \ \exp(-\gamma z) \tag{6}$$

where

$$[N] = \begin{bmatrix} \{N\} & \{0\} & \{0\} \\ \{0\} & \{N\} & \{0\} \\ \{0\} & \{0\} & j\{N\} \end{bmatrix} \tag{7}$$

and

$$\{H\}_e = \begin{bmatrix} \{H_x\}_e \\ \{H_y\}_e \\ \{H_z\}_e \end{bmatrix}. \tag{8}$$

Here, $\{N\}$ is the shape function vector; $\{0\}$ is a null vector; T, $\{\cdot\}$, and $\{\cdot\}^T$ denote a transposition, a column vector, and a row vector, respectively; and $\{H_x\}_e$, $\{H_y\}_e$, and $\{H_z\}_e$ are complex magnetic-field vectors corresponding to the nodal points within each element e.

Application of the standard finite-element technique via a Galerkin procedure to (3) gives the following global matrix equation:

$$[S]\{H\} + k_0[T']\{H\} - k_0^2[T]\{H\} = \{0\} \tag{9}$$

where

$$[S] = \sum_e \iint_e [B'(\gamma)][\epsilon]_e^{-1}[B(\gamma)]^T dx\,dy \tag{10}$$

$$[T'] = j(Z_n/Z_0)\sum_{e'} \int_{e'} [N]^*[N(\theta)]^T d\Gamma \tag{11}$$

$$[T] = \sum_e \iint_e [N]^*[N]^T dx\,dy \qquad (*\text{: complex conjugate}) \tag{12}$$

$$[B(\gamma)] = \begin{bmatrix} \{0\} & -\gamma\{N\} & -\partial\{N\}/\partial y \\ \gamma\{N\} & \{0\} & \partial\{N\}/\partial x \\ j\partial\{N\}/\partial y & -j\partial\{N\}/\partial x & \{0\} \end{bmatrix} \tag{13a}$$

$$[B'(\gamma)] = \begin{bmatrix} \{0\} & \gamma\{N\} & -\partial\{N\}/\partial y \\ -\gamma\{N\} & \{0\} & \partial\{N\}/\partial x \\ -j\partial\{N\}/\partial y & j\partial\{N\}/\partial x & \{0\} \end{bmatrix} \tag{13b}$$

$$[N(\theta)] = \begin{bmatrix} \sin^2\theta\{N\} & -\sin\theta\cos\theta\{N\} & \{0\} \\ -\sin\theta\cos\theta\{N\} & \cos^2\theta\{N\} & \{0\} \\ \{0\} & \{0\} & j\{N\} \end{bmatrix}. \tag{14}$$

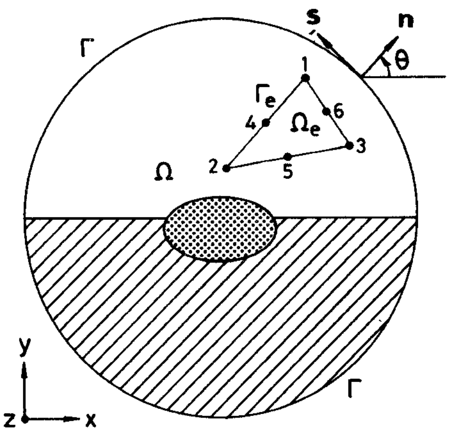

Fig. 1. Geometry of problem. $\boldsymbol{n}$: unit normal vector; $\boldsymbol{s}$: unit tangential vector; θ: angle between $\boldsymbol{n}$ and x axis; Ω: waveguide cross section; Γ: impedance wall.

Here, Σ_e and $\Sigma_{e'}$ stand for summation over all elements related to the domain Ω and the boundary Γ, respectively, and Z_n and Z_0 are the surface impedance [11] of Γ and the intrinsic impedance of vacuum, respectively. (The derivation of (9) is given in Appendix I.) Provided that Γ is a perfect electric or magnetic wall, the second term of the left-hand side of (9) is dropped [12].

The solutions of (9) are known to involve many spurious solutions which do not satisfy the divergence relation (4) [12]. In what follows, we adopt the same procedure developed for the loss-free system in [10] to avoid such unnecessary solutions.

Using the finite-element method based on a Galerkin procedure on (4), the following matrix relation is obtained [10]:

$$\{H\} = [D]\{H_t\} \tag{15}$$

where

$$[D] = \begin{bmatrix} [U] \\ [D_z]^{-1}[D_t] \end{bmatrix} \tag{16}$$

$$[D_z] = \sum_e \iint_e \{N\}\{N\}^T dx\,dy \tag{17}$$

$$[D_t] = -j\gamma^{-1}\sum_e \iint_e \left[\{N\}\partial\{N\}^T/\partial x \quad \{N\}\partial\{N\}^T/\partial y\right] dx\,dy \tag{18}$$

$$\{H_t\} = \begin{bmatrix} \{H_x\} \\ \{H_y\} \end{bmatrix}. \tag{19}$$

Here, the components of vectors $\{H_x\}$ and $\{H_y\}$ are the values of H_x and H_y at nodal points in Ω, respectively, and $[U]$ is a unit matrix.

Substituting (15) into (9) and operating $[D]^T$ on the left [10], the following matrix equation with the complex transverse magnetic-field component $\{H_t\}$ is derived:

$$[\tilde{S}_{tt}]\{H_t\}+k_0[\tilde{T}'_{tt}]\{H_t\}-k_0^2[\tilde{T}_{tt}]\{H_t\}=\{0\} \quad (20)$$

where

$$[\tilde{S}_{tt}]=[D]^T[S][D] \quad (21)$$

$$[\tilde{T}'_{tt}]=[D]^T[T'][D] \quad (22)$$

$$[\tilde{T}_{tt}]=[D]^T[T][D]. \quad (23)$$

Note that in (20) the divergence relation (4) is considered [10]. However, (20) is a matrix eigenvalue problem whose eigenvalue corresponds to k_0; it is therefore necessary to iterate on α or β until the imaginary part of k_0 becomes negligible. Similarly, the imaginary part of the dielectric, which depends on ω, will need to be iterated until $\epsilon''=\sigma/\omega$ for a medium of relative conductivity σ. To avoid such inefficiency, in what follows we modify (20) into a convenient form to be γ^2 as an eigenvalue.

Substituting (10)–(12) and (16)–(18) into (20)–(23) and rearranging (20) into a desirable form, the following final matrix equation is derived:

$$\lambda^2[A]\{H_t\}+\lambda[B]\{H_t\}+[C]\{H_t\}=\{0\} \quad (24)$$

where

$$\lambda=-\gamma^2 \quad (25)$$

$$[A]=\begin{bmatrix}[G_6^y] & [0]\\ [0]^T & [G_6^x]\end{bmatrix} \quad ([0]\text{: null matrix}) \quad (26)$$

$$[B]=\begin{bmatrix}[B_{xx}] & [B_{xy}]\\ [B_{xy}]^T & [B_{yy}]\end{bmatrix} \quad (27)$$

Here, $[G_1]$–$[G_6]$, $[G_6']$, and $[G_1^i]$–$[G_6^i]$ $(i=x,y,z)$ are defined by

$$[G_1]=\sum_e\iint_e(\partial\{N\}/\partial x)(\partial\{N\}^T/\partial x)\,dx\,dy \quad (35)$$

$$[G_2]=\sum_e\iint_e(\partial\{N\}/\partial y)(\partial\{N\}^T/\partial y)\,dx\,dy \quad (36)$$

$$[G_3]=\sum_e\iint_e(\partial\{N\}/\partial x)(\partial\{N\}^T/\partial y)\,dx\,dy \quad (37)$$

$$[G_4]=\sum_e\iint_e(\partial\{N\}/\partial x)\{N\}^T\,dx\,dy \quad (38)$$

$$[G_5]=\sum_e\iint_e(\partial\{N\}/\partial y)\{N\}^T\,dx\,dy \quad (39)$$

$$[G_6]=\sum_e\iint_e\{N\}\{N\}^T\,dx\,dy \quad (40)$$

$$[G_6']=\sum_{e'}\int_{e'}\{N\}\{N\}^T\,d\Gamma \quad (41)$$

$$[G_1^i]=\sum_e\iint_e\epsilon_{i,e}^{-1}(\partial\{N\}/\partial x)(\partial\{N\}^T/\partial x)\,dx\,dy \quad (42)$$

$$[G_2^i]=\sum_e\iint_e\epsilon_{i,e}^{-1}(\partial\{N\}/\partial y)(\partial\{N\}^T/\partial y)\,dx\,dy \quad (43)$$

$$[G_3^i]=\sum_e\iint_e\epsilon_{i,e}^{-1}(\partial\{N\}/\partial x)(\partial\{N\}^T/\partial y)\,dx\,dy \quad (44)$$

$$[G_4^i]=\sum_e\iint_e\epsilon_{i,e}^{-1}(\partial\{N\}/\partial x)\{N\}^T\,dx\,dy \quad (45)$$

$$[G_5^i]=\sum_e\iint_e\epsilon_{i,e}^{-1}(\partial\{N\}/\partial y)\{N\}^T\,dx\,dy \quad (46)$$

$$[G_6^i]=\sum_e\iint_e\epsilon_{i,e}^{-1}\{N\}\{N\}^T\,dx\,dy. \quad (47)$$

The derivation of (24) is given in Appendix II.

$$[B_{xx}]=[G_2^z]-[G_4^y]^T[G_6]^{-1}[G_4]^T-[G_4][G_6]^{-1}[G_4^y]-k_0^2[G_6]+k_0(jZ_n/Z_0)\sin^2\theta[G_6'] \quad (28)$$

$$[B_{xy}]=-[G_3^z]^T-[G_4^y]^T[G_6]^{-1}[G_5]^T-[G_4][G_6]^{-1}[G_5^x]-k_0(jZ_n/Z_0)\sin\theta\cos\theta[G_6'] \quad (29)$$

$$[B_{yy}]=[G_1^z]-[G_5^x]^T[G_6]^{-1}[G_5]^T-[G_5][G_6]^{-1}[G_5^x]-k_0^2[G_6]+k_0(jZ_n/Z_0)\cos^2\theta[G_6'] \quad (30)$$

$$[C]=\begin{bmatrix}[C_{xx}] & [C_{xy}]\\ [C_{xy}]^T & [C_{yy}]\end{bmatrix} \quad (31)$$

$$[C_{xx}]=[G_4][G_6]^{-1}([G_1^y]+[G_2^x])[G_6]^{-1}[G_4]^T-k_0^2[G_4][G_6]^{-1}[G_4]^T+k_0(jZ_n/Z_0)[G_4][G_6]^{-1}[G_6'][G_6]^{-1}[G_4]^T \quad (32)$$

$$[C_{xy}]=[G_4][G_6]^{-1}([G_1^y]+[G_2^x])[G_6]^{-1}[G_5]^T-k_0^2[G_4][G_6]^{-1}[G_5]^T+k_0(jZ_n/Z_0)[G_4][G_6]^{-1}[G_6'][G_6]^{-1}[G_5]^T \quad (33)$$

$$[C_{yy}]=[G_5][G_6]^{-1}([G_1^y]+[G_2^x])[G_6]^{-1}[G_5]^T-k_0^2[G_5][G_6]^{-1}[G_5]^T+k_0(jZ_n/Z_0)[G_5][G_6]^{-1}[G_6'][G_6]^{-1}[G_5]^T. \quad (34)$$

Since (24) is a complex quadratic eigenvalue problem, it can be reduced to the following standard form [13]:

$$\begin{bmatrix} [0] & [U] \\ -[A]^{-1}[C] & -[A]^{-1}[B] \end{bmatrix} \begin{bmatrix} \{H_t\} \\ \{\bar{H}_t\} \end{bmatrix} = \lambda \begin{bmatrix} \{H_t\} \\ \{\bar{H}_t\} \end{bmatrix} \quad (48)$$

where

$$\{\bar{H}_t\} = \lambda \{H_t\}. \quad (49)$$

Although (48) shows a little complexity in comparison with previous formulations [2]–[5], it is a standard eigenvalue problem whose eigenvalue directly corresponds to the propagation constant γ. Thus, one can avoid unnecessary iterations using complex frequencies. The only disadvantage of this form is that it involves $4N_P$ unknown components in each eigenvector compared with $2N_P$ components in the original system, where N_P is the number of nodal points.

IV. Numerical Examples

In this section, we present computed results obtained by (48). In numerical computations, the HITAC S-810/10 supercomputer is used and double precision is adopted to avoid roundoff errors. The inverse matrices, $[G_6]^{-1}$ and $[A]^{-1}$, are computed via the Gauss–Jordan method. As an eigenvalue solution method, the LR algorithm is applied; eigenvectors are computed via the inverse iteration.

A. Dielectric-Filled Rectangular Waveguide

Fig. 2(a) shows the relative error of the computed propagation constant for the fundamental (TE_{10}) and first higher order (TE_{01}) modes in a rectangular metallic waveguide filled with lossy isotropic dielectric of relative permittivity $\epsilon = 1.5 - j1.5$. Four divisions, $(N_E, N_P) = (4,15)$, (16,45), (36,91), and (64,153), are chosen in the numerical computations, and storage requirements are 0.3, 2.4, 9.6, and 27.0 MB, respectively.

The relative error e is defined by

$$e = \begin{cases} (\alpha - \bar{\alpha})/\bar{\alpha} & \text{for attenuation constant} \\ (\beta - \bar{\beta})/\bar{\beta} & \text{for phase constant} \end{cases} \quad (50)$$

where (α, β) and $(\bar{\alpha}, \bar{\beta})$ are the computed and exact solutions, respectively. The exact solutions are

$$\bar{\beta}/k_0 = \left[\left\{p + (p^2 + q^2)^{1/2}\right\}/2\right]^{1/2} \quad (51)$$

$$\bar{\alpha}/k_0 = (q/2)(\bar{\beta}/k_0)^{-1} \quad (52)$$

where

$$p = \epsilon' - \{m\pi/(k_0 a)\}^2 - \{n\pi/(k_0 b)\}^2, \qquad q = \epsilon''. \quad (53)$$

Here, m and n stand for the mode indices for the x and y directions, respectively.

It is readily seen from Fig. 2(a) that the relative error decreases as the number of elements N_E increases. Also, it is interesting to note that the directions of convergence are opposite between the real and imaginary parts of the propagation constant; i.e., $e > 0$ for α whereas $e < 0$ for β. Investigation of the near-cutoff frequency for the TE_{10} mode ($k_0 b = 0.01$) has been carried out as well. Also in this case, the relative error decreases as N_E increases. However, the same direction of convergence, $e < 0$, is observed for both α and β.

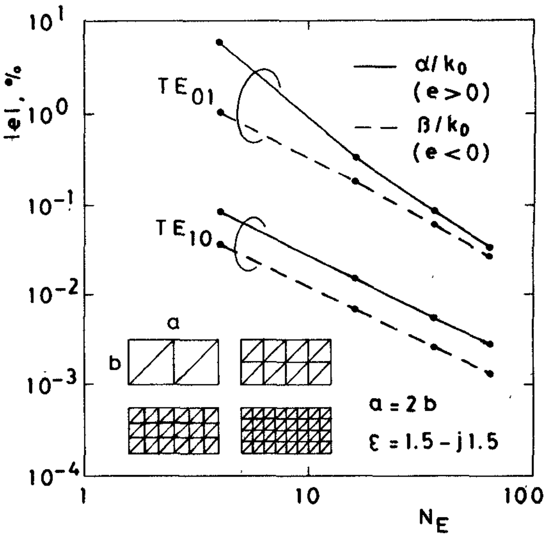

(a)

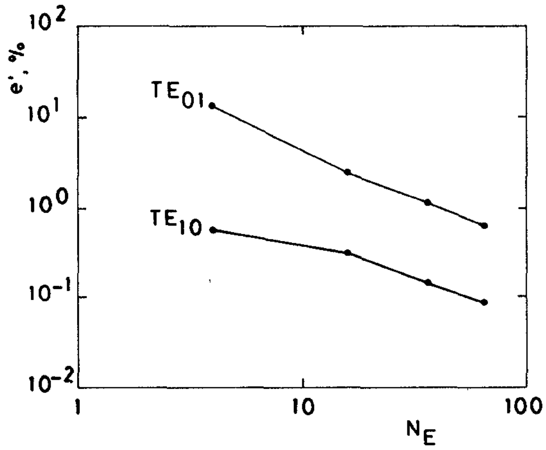

(b)

Fig. 2. Convergence of solutions ($k_0 b = 3.0$). (a) Eigenvalues. (b) Eigenvectors.

Fig. 2(b) shows the relative error of the computed eigenvectors for Fig. 2(a). Since exact analytical solutions give $H_y \equiv 0$ and $H_x \equiv 0$ for the TE_{10} and TE_{01} modes, respectively, the following definitions are adopted as a measure of error involved in eigenvectors:

$$e' = \begin{cases} \|H_y\|/\|H_x\| & \text{for } TE_{10} \text{ mode} \\ \|H_x\|/\|H_y\| & \text{for } TE_{01} \text{ mode} \end{cases} \quad (54)$$

$$\|H_i\| = \sqrt{\{H_i\}^\dagger \{H_i\}} \qquad (i = x, y) \quad (55)$$

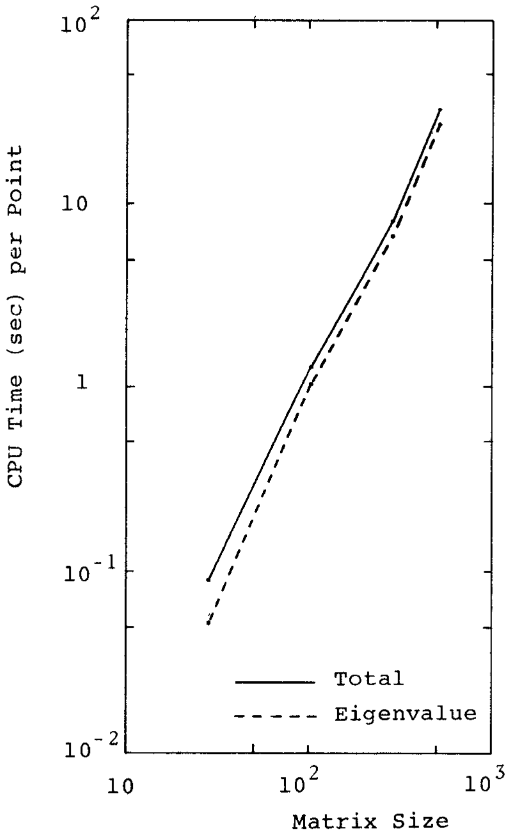

Fig. 3. Computing time necessary to obtain one point in propagation diagram. The solid line shows total CPU time, whereas the broken line shows CPU time necessary to solve the eigenvalue problem (48).

where † denotes complex conjugate and transpose. It is found from Fig. 2(b) that the relative error decreases as N_E increases.

Fig. 3 displays the computing time necessary to obtain one point in a propagation diagram, where the abscissa means the dimension of the final matrix equation (48). Comparison between the solid and broken lines indicates that in the present program the greater part of the computing time is spent on solving (48).

B. Shielded Image Guide

As an advanced application of the present program, we next consider a lossy image guide shielded with a perfectly conducting box ($Z_n = 0$). We subdivide only half of the cross section of a guide into second-order triangular elements; the plane of symmetry is assumed to be a magnetic wall. The storage requirement is 7.6 MB in this division.

Fig. 4 shows the dispersion characteristics in the slow-wave region for the E_{11}^y mode of a lossy isotropic image guide, taking the imaginary part of relative permittivity, ϵ'', as a parameter. As is seen from Fig. 4(a), the phase constant β for $\epsilon'' = 0.15$ (loss tangent: $\tan\delta = 0.1$) is almost the same as that for $\epsilon'' = 0$, i.e., the loss-free case.

Since the relative permittivity tensor assumed in this paper is arbitrarily diagonal as shown in (1), we can consider a lossy anisotropic waveguide whose principal axis coincides with one of the coordinate axes.

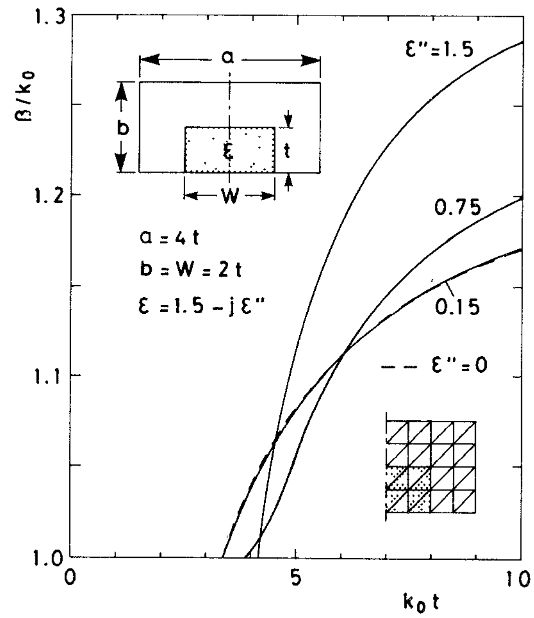

(a)

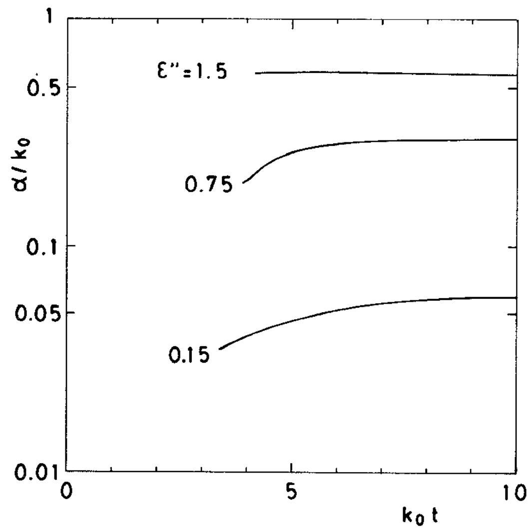

(b)

Fig. 4. Dispersion characteristics for shielded image guide composed of lossy isotropic dielectric (E_{11}^y mode). (a) Normalized phase constant. (b) Normalized attenuation constant.

Figs. 5 and 6 show the dispersion characteristics in the slow-wave region for the E_{11}^y mode of a lossy anisotropic image guide whose cross-sectional shape is the same as that in Fig. 4. The real part of ϵ_y, ϵ_y', is chosen as a parameter in Fig. 5 ("dielectric anisotropy"), whereas the imaginary part of ϵ_y, ϵ_y'', is chosen in Fig. 6 ("conductivity anisotropy"). Comparison between Fig. 5(a) and Fig. 6(a) clearly shows that a similar effect is seen in the phase behavior from the two types of anisotropy. On the contrary, as is found from the comparison between Fig. 5(b) and Fig. 6(b), the opposite effect is seen in the attenuation behavior from the above two types of anisotropy. That is, the attenuation becomes smaller as ϵ_y' increases while it becomes larger as ϵ_y'' increases.

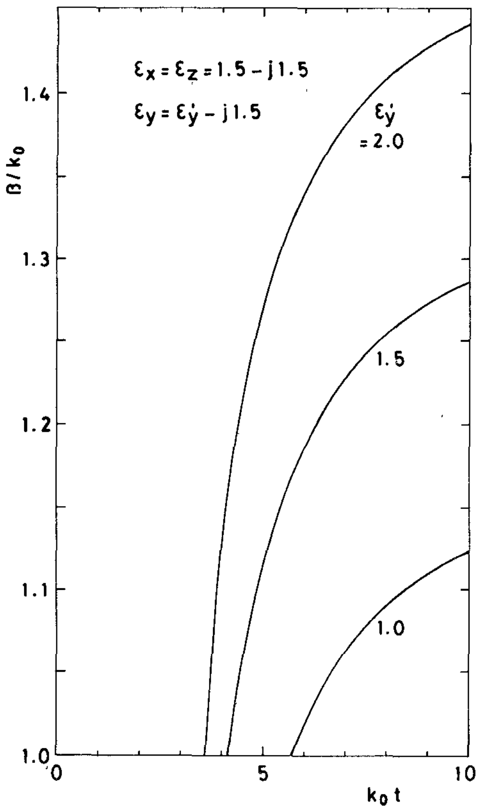

(a)

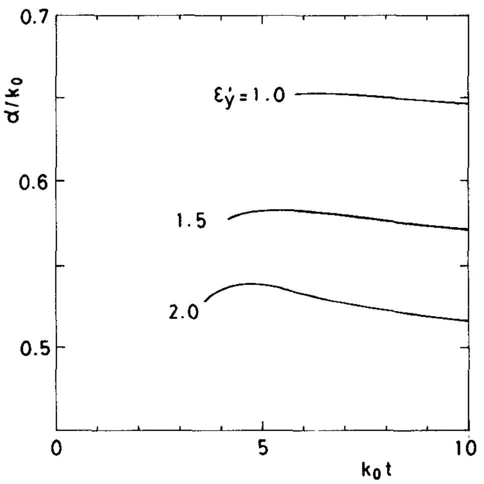

(b)

Fig. 5. Dispersion characteristics for shielded image guide composed of lossy anisotropic dielectric (E_{11}^y mode). The real part of dielectric is assumed to be anisotropic. (a) Normalized phase constant. (b) Normalized attenuation constant.

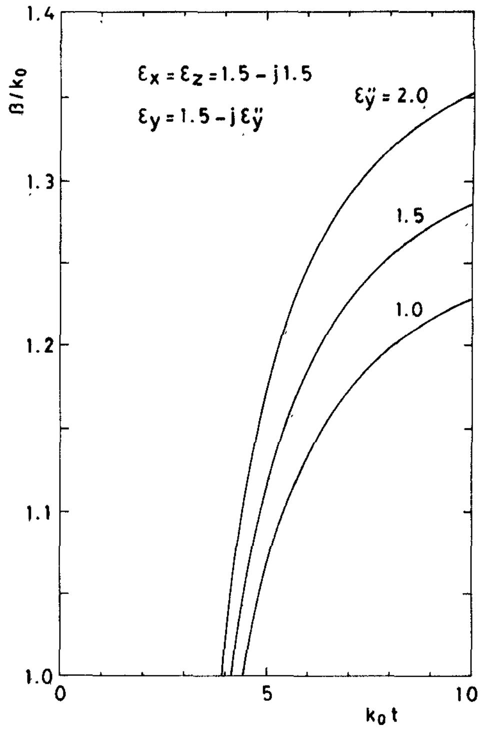

(a)

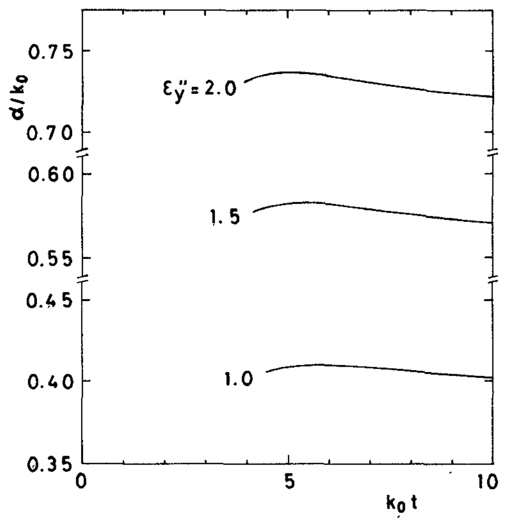

(b)

Fig. 6. Dispersion characteristics for shielded image guide composed of lossy anisotropic dielectric (E_{11}^y mode). The imaginary part of dielectric is assumed to be anisotropic. (a) Normalized phase constant. (b) Normalized attenuation constant.

C. Dielectric-Loaded Waveguide with Impedance Walls

As an example of the guide with the impedance walls characterized by the surface impedance, we consider a dielectric-loaded waveguide surrounded by a medium with the surface impedance Z_n. We subdivide the entire cross section of the guide into second-order triangular elements ($N_E = 16$, $N_p = 45$); the storage requirement is 2.5 MB.

Fig. 7 shows the dispersion characteristics for the first five modes of a lossy dielectric-loaded rectangular waveguide with impedance walls ($Z_n/Z_0 = 10^{-3}(1+j)$). Our results agree well with those computed by Matsuhara *et al.* [8] for both attenuation and phase.

V. Conclusions

A powerful computer-aided solution procedure based on the finite-element method has been developed for solving general waveguiding structures composed of arbitrarily lossy media. In this procedure, a formulation in terms of

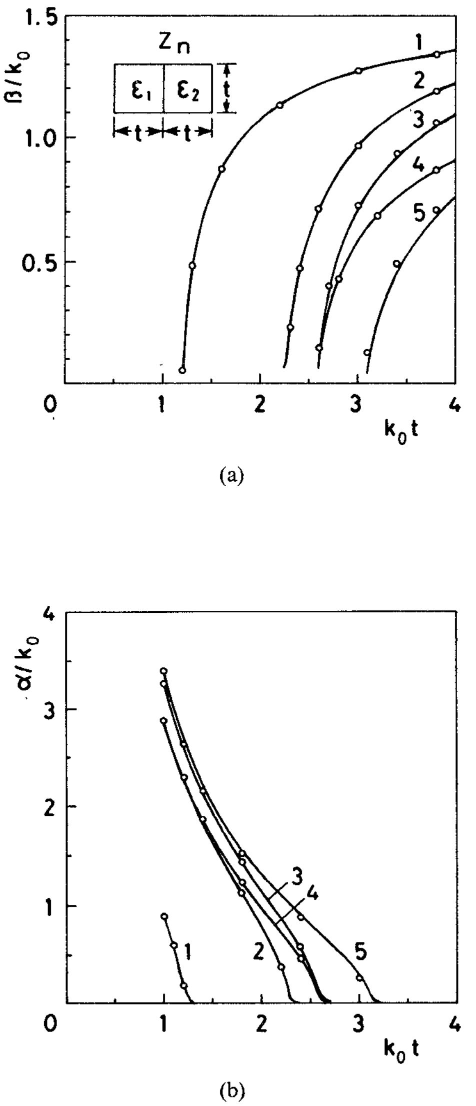

Fig. 7. Dispersion characteristics for lossy dielectric-loaded waveguide with impedance walls. $\epsilon_1 = 2.25(1-j0.01)$, $\epsilon_2 = 1.0$, $Z_n/Z_0 = 10^{-3}(1+j)$. —present method; ° Matsuhara *et al.* (a) Normalized phase constant. (b) Normalized attenuation constant.

transverse magnetic-field component established for a general loss-free system has been extended to a lossy system. The main advantage of the present scheme is that one can avoid the unnecessary iteration by means of complex frequencies because the eigenvalue of the final matrix equation to be solved corresponds to the propagation constant itself.

Although we have considered dielectric waveguides within a conducting box, one can straightforwardly apply the present approach to open, unbounded dielectric waveguides with the help of the virtual boundary walls [6], [7], [10], [12] or the infinite elements [14]. Application to the case of curved metallic boundaries is also straightforward provided that they are replaced by a number of straight lines and appropriate boundary conditions [15] are imposed on each line. Furthermore, the present method can be extended to the case of arbitrary permittivity tensor with off-diagonal elements.

Appendix I
Derivation of (9)

Application of the standard finite-element method [12] based on a Galerkin procedure to (3) yields the following matrix equation including boundary integral term along Γ:

$$[S]\{H\} - k_0^2[T]\{H\} + j(k_0/Z_0) \cdot \int_\Gamma (e^{\gamma z}[N]^*)(\boldsymbol{n}\times\boldsymbol{E})\,d\Gamma = \{0\} \quad \text{(A1)}$$

where the Maxwell's curl equation

$$\nabla\times\boldsymbol{H} = j\omega\epsilon_0[\epsilon]\boldsymbol{E} \qquad (\epsilon_0\text{: vacuum permittivity}) \quad \text{(A2)}$$

has been utilized.

If a highly conductive material is assumed outside Γ, the following boundary conditions derived from the plane-wave approximation [11] hold:

$$E_s = Z_n H_z, \qquad E_z = -Z_n H_s \qquad \text{on } \Gamma. \quad \text{(A3)}$$

Using (A3), $\boldsymbol{n}\times\boldsymbol{E}$ in (A1) is evaluated as

$$\begin{aligned}\boldsymbol{n}\times\boldsymbol{E} &= Z_n(\boldsymbol{s}H_s + \boldsymbol{z}H_z)\\ &= Z_n\Big\{\boldsymbol{x}\big(H_x\sin^2\theta - H_y\sin\theta\cos\theta\big)\\ &\quad + \boldsymbol{y}\big(-H_x\sin\theta\cos\theta\\ &\quad + H_y\cos^2\theta\big) + \boldsymbol{z}H_z\Big\}\end{aligned} \quad \text{(A4)}$$

where

$$\boldsymbol{s} = -\boldsymbol{x}\sin\theta + \boldsymbol{y}\cos\theta \quad \text{(A5)}$$

and

$$H_s = -H_x\sin\theta + H_y\cos\theta \quad \text{(A6)}$$

have been used. Here, $\boldsymbol{x}$, $\boldsymbol{y}$, and $\boldsymbol{z}$ are unit vectors for x, y, and z directions, respectively.

Substituting (6) into (A4) and (A1), (9) is derivable.

Appendix II
Derivation of (24)

Using the notations (35)–(47), $[S]$, $[T']$, and $[T]$ are explicitly written as

$$[S] = \begin{bmatrix} [S_{tt}] & [S_{tz}] \\ [S_{tz}]^T & [S_{zz}] \end{bmatrix} \quad \text{(A7)}$$

$$[S_{tt}] = \begin{bmatrix} [S_{xx}] & [S_{xy}] \\ [S_{xy}]^T & [S_{yy}] \end{bmatrix}, \qquad [S_{tz}] = \begin{bmatrix} [S_{xz}] \\ [S_{yz}] \end{bmatrix} \quad \text{(A8)}$$

$$[S_{xx}] = [G_2^z] - \gamma^2[G_6^y] \quad \text{(A9)}$$

$$[S_{xy}] = -[G_3^z]^T \quad \text{(A10)}$$

$$[S_{yy}] = [G_1^z] - \gamma^2 [G_6^x] \tag{A11}$$

$$[S_{xz}] = -j\gamma [G_4^y]^T \tag{A12}$$

$$[S_{yz}] = -j\gamma [G_5^x]^T \tag{A13}$$

$$[S_{zz}] = [G_1^y] + [G_2^x] \tag{A14}$$

$$[T'] = \begin{bmatrix} [T'_{tt}] & [0] \\ [0]^T & [T'_{zz}] \end{bmatrix} \tag{A15}$$

$$[T'_{tt}] = \begin{bmatrix} [T'_{xx}] & [T'_{xy}] \\ [T'_{xy}]^T & [T'_{yy}] \end{bmatrix} \tag{A16}$$

$$[T'_{xx}] = j(Z_n/Z_0)\sin^2\theta[G'_6] \tag{A17}$$

$$[T'_{xy}] = -j(Z_n/Z_0)\sin\theta\cos\theta[G'_6] \tag{A18}$$

$$[T'_{yy}] = j(Z_n/Z_0)\cos^2\theta[G'_6] \tag{A19}$$

$$[T'_{zz}] = j(Z_n/Z_0)[G'_6] \tag{A20}$$

$$[T] = \begin{bmatrix} [T_{tt}] & [0] \\ [0]^T & [T_{zz}] \end{bmatrix} \tag{A21}$$

$$[T_{tt}] = \begin{bmatrix} [T_{xx}] & [0] \\ [0]^T & [T_{yy}] \end{bmatrix} \tag{A22}$$

$$[T_{xx}] = [T_{yy}] = [T_{zz}] = [G_6]. \tag{A23}$$

Similarly, $[D_t]$ and $[D_z]$ in (16) are

$$[D_t] = -j\gamma^{-1}\left[[G_4]^T \quad [G_5]^T\right] \tag{A24}$$

$$[D_z] = [G_6]. \tag{A25}$$

Substituting (16), (A7), (A15), and (A21) into (21)–(23), we can obtain

$$[\tilde{S}_{tt}] = [S_{tt}] + [S_{tz}][D_z]^{-1}[D_t] + \left([S_{tz}][D_z]^{-1}[D_t]\right)^T + [D_t]^T[D_z]^{-1}[S_{zz}][D_z]^{-1}[D_t] \tag{A26}$$

$$[\tilde{T}'_{tt}] = [T'_{tt}] + [D_t]^T[D_z]^{-1}[T'_{zz}][D_z]^{-1}[D_t] \tag{A27}$$

$$[\tilde{T}_{tt}] = [T_{tt}] + [D_t]^T[D_z]^{-1}[T_{zz}][D_z]^{-1}[D_t]. \tag{A28}$$

Substituting (A8)–(A14), (A16)–(A20), and (A22)–(A25) into (A26)–(A28) and (20), and rearranging the left-hand side of (20) as a polynomial of γ^2, we can derive (24).

Acknowledgment

The authors would like to express their gratitude to the late Professor Michio Suzuki of Hokkaido University for his advice and encouragement during his lifetime. They would also like to thank Dr. M. Matsuhara of Osaka University for presenting them with his computed data of Fig. 7.

References

[1] S. M. Saad, "Review of numerical methods for the analysis of arbitrarily-shaped microwave and optical dielectric waveguides," *IEEE Trans. Microwave Theory Tech.*, vol. MTT-33, pp. 894–899, Oct. 1985.

[2] A. D. McAulay, "Variational finite-element solution for dissipative waveguides and transportation application," *IEEE Trans. Microwave Theory Tech.*, vol. MTT-25, pp. 382–392, May 1977.

[3] A. D. McAulay, "The finite element solution of dissipative electromagnetic surface waveguides," *Int. J. Numer. Meth. Engrg.*, vol. 11, pp. 11–25, 1977.

[4] M. Aubourg, J.-P. Villotte, F. Godon, and Y. Garault, "Finite element analysis of lossy waveguides—Application to microstrip lines on semiconductor substrate," *IEEE Trans. Microwave Theory Tech.*, vol. MTT-31, pp. 326–331, Apr. 1983.

[5] C.-K. Tzuang and T. Itoh, "Finite-element analysis of slow-wave Schottky contact printed lines," *IEEE Trans. Microwave Theory Tech.*, vol. MTT-34, pp. 1483–1489, Dec. 1986.

[6] K. Hayata, M. Koshiba, and M. Suzuki, "Analysis of partially metal-clad and dielectric overlay-loaded diffused optical waveguide," *Electron. Commun. Japan*, vol. 67, pp. 108–116, May 1984.

[7] K. Hayata, M. Koshiba, and M. Suzuki, "Lateral mode analysis of buried heterostructure diode lasers by the finite-element method," *IEEE J. Quantum Electron.*, vol. QE-22, pp. 781–788, June 1986.

[8] M. Matsuhara, T. Angkaew, and N. Kumagai, "Analysis of the waveguide with loss or gain by the finite-element method," (in Japanese) in *Proc. 8th Symp. Appl. FEM to Electrical and Electronic Engrg.* (Tokyo, Japan), Mar. 1987, pp. 141–146.

[9] T. Angkaew, M. Matsuhara, and N. Kumagai, "Finite-element analysis of waveguide modes: A novel approach that eliminates spurious modes," *IEEE Trans. Microwave Theory Tech.*, vol. MTT-35, pp. 117–123, Feb. 1987.

[10] K. Hayata, M. Koshiba, M. Eguchi, and M. Suzuki, "Vectorial finite-element method without any spurious solutions for dielectric waveguiding problems using transverse magnetic-field component," *IEEE Trans. Microwave Theory Tech.*, vol. MTT-34, pp. 1120–1124, Nov. 1986.

[11] K. Yasumoto and H. Shigematsu, "Analysis of propagation characteristics of radio waves in tunnels using a surface impedance approximation," *Radio Sci.*, vol. 19, pp. 597–602, Mar.–Apr. 1984.

[12] M. Koshiba, K. Hayata, and M. Suzuki, "Vectorial finite-element formulation without spurious modes for dielectric waveguides," *Trans. IECE Japan*, vol. E67, pp. 191–196, Apr. 1984.

[13] D. A. Gignac, "Solution of a complex quadratic eigenvalue problem," *Int. J. Numer. Meth. Engrg.*, vol. 11, pp. 99–106, 1977.

[14] P. Bettess, "Infinite elements," *Int. J. Numer. Meth. Engrg.*, vol. 11, pp. 53–64, 1977.

[15] M. Koshiba, K. Hayata, and M. Suzuki, "Improved finite-element formulation in terms of the magnetic-field vector for dielectric waveguides," *IEEE Trans. Microwave Theory Tech.*, vol. MTT-33, pp. 227–233, Mar. 1985.

Kazuya Hayata was born in Kushiro, Japan, on December 1, 1959. He received the B.S. and M.S. degrees in electronic engineering from Hokkaido University, Sapporo, Japan, in 1982 and 1984, respectively.

Since 1984, he has been an Instructor of Electronic Engineering at Hokkaido University. He has been engaged in research on guided-wave optics, microwave theory and techniques, computational mechanics for field problems, quantum-wave electronics, and surface acoustic waves.

Mr. Hayata is a member of the Institute of Electronics, Information and Communication Engineers (IEICE), the Japan Society of Applied Physics (JSAP), and the Optics Division in the JSAP. In 1987, he was awarded the 1986 Paper Award by the IEICE.

Kazunori Miura was born in Abuta, Hokkaido, Japan, on July 17, 1963. He received the B.S. degree in electronic engineering from Hokkaido University, Sapporo, Japan, in 1986. He is presently studying toward the M.S. degree in electronic engineering at Hokkaido University.

Mr. Miura is a member of the Institute of Electronics, Information and Communication Engineers.

Masanori Koshiba (SM'84) was born in Sapporo, Japan, on November 23, 1948. He received the B.S., M.S., and Ph.D. degrees in electronic engineering from Hokkaido University, Sapporo, Japan, in 1971, 1973, and 1976, respectively.

In 1976, he joined the Department of Electronic Engineering, Kitami Institute of Technology, Kitami, Japan. From 1979 to 1987, he was an Associate Professor of Electronic Engineering at Hokkaido University, and in 1987 he became a Professor. He has been engaged in research on lightwave technology, surface acoustic waves, magnetostatic waves, microwave field theory, and applications of finite-element and boundary-element methods to field problems.

Dr. Koshiba is a member of the Institute of Electronics, Information and Communication Engineers (IEICE), the Institute of Television Engineers of Japan, the Institute of Electrical Engineers of Japan, the Japan Society for Simulation Technology, and the Japan Society for Computational Methods in Engineering. In 1987, he was awarded the 1986 Paper Award by the IEICE.